

See discussions, stats, and author profiles for this publication at: <https://www.researchgate.net/publication/51839618>

# Size-Dependent Properties of Small Unilamellar Vesicles Formed by Model Lipids

ARTICLE *in* LANGMUIR · NOVEMBER 2011

Impact Factor: 4.46 · DOI: 10.1021/la203755v · Source: PubMed

---

CITATIONS

23

READS

17

## 5 AUTHORS, INCLUDING:



David Wu

Colorado School of Mines

98 PUBLICATIONS 1,666 CITATIONS

SEE PROFILE

## Size-Dependent Properties of Small Unilamellar Vesicles Formed by Model Lipids

Chun-Min Lin

Institute of Polymer Science and Engineering, National Taiwan University, Taipei, Taiwan 106, R.O.C.

Chun-Shian Li and Yu-Jane Sheng\*

Department of Chemical Engineering, National Taiwan University, Taipei, Taiwan 106, R.O.C.

David T. Wu

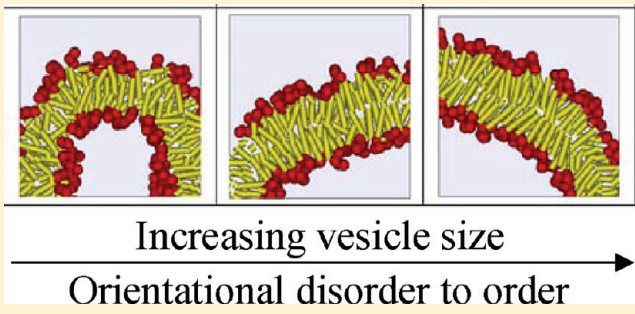
Department of Chemical Engineering and Department of Chemistry, Colorado School of Mines, Golden, Colorado 80401, United States

Heng-Kwong Tsao\*

Department of Chemical and Materials Engineering, Department of Physics, National Central University, Jhongli, Taiwan 320, R.O.C.

 Supporting Information

**ABSTRACT:** The size-dependent behavior of small unilamellar vesicles is explored by dissipative particle dynamics, including the membrane characteristics and mechanical properties. The spontaneously formed vesicles are in the metastable state and the vesicle size is controlled by the concentration of model lipids. As the vesicle size decreases, the bilayer gets thinner and the area density of heads declines. Nonetheless, the area density in the inner leaflet is higher than that in the outer. The packing parameters are calculated for both leaflets. The result indicates that the shape of lipid in the outer leaflet is like a truncated cone but that in the inner leaflet resembles an inverted truncated cone. Based on a local order parameter, our simulations indicate that the orientation order of lipid molecules decreases as the size of the vesicle reduces and this fact reveals that the bilayer becoming thinner for smaller vesicle is mainly attributed to the orientation disorder of the lipids. The membrane tension can be obtained through the Young–Laplace equation. The tension is found to grow with reducing vesicle size. Therefore, small vesicles are less stable against fusion. Using the inflation method, the area stretching and bending moduli can be determined and those moduli are found to grow with reducing size. Nonetheless, a general equation with a single numerical constant can relate bending modulus, area stretching modulus, and bilayer thickness irrespective of the vesicle size. Finally, a simple metastable model is proposed to explain the size-dependent behavior of bilayer thickness, orientation, and tension.



### I. INTRODUCTION

The membrane vesicles are self-assembly structures consisting of bilayers of fluid lipids or amphiphilic block copolymers, which roll up into a spherical shell, enclosing a small amount of water and separating it from the water outside the vesicle.<sup>1–4</sup> In living cells, vesicles can transport lipids, proteins, and many other molecules within the cell as well as into or out of the cell. The naturally formed vesicles consist of a complex mixture of different lipids and proteins. Although they offer greater realism for studying specific biological phenomena, simple artificial vesicles have been extensively used for studies of fundamental bilayer properties owing to their fundamental similarity to the cell membrane. Another reason vesicles have been used so frequently is that they are relatively easy to make.

Phospholipid vesicles, also known as liposomes, of various sizes and compositions have been employed as carriers, both in vitro and in vivo, to introduce biologically active substances into cells. Polymersomes are similar to liposomes and assembled by amphiphilic synthetic block copolymers.<sup>5,6</sup> Most reported polymersomes contain an aqueous solution in their core and are useful for encapsulating and protecting sensitive molecules, including drugs, enzymes, peptides, and DNA and RNA fragments. While having many of the properties of natural liposomes, polymersomes exhibit increased stability and reduced permeability. Furthermore,

**Received:** September 25, 2011

**Revised:** November 28, 2011

**Published:** November 29, 2011

the use of synthetic polymers enables designers to manipulate the membrane characteristics and thus control stability, permeability, and other properties of the vesicles. The deployment of medicines to specifically targeted parts of our bodies is the goal of all drug delivery systems. Liposomes or polymersomes have been shown to be able to not only provide protections for drugs against biochemical degradation, but also effectively enhance drug targeting specificity. As a consequence, artificial membrane vesicles are extensively utilized as carriers for drug delivery systems to improve absorption rates, and the properties of the bilayer membrane play a key role in their performance.

At a given temperature, a lipid bilayer behaves like either a liquid or a solid phase, and therefore, it can exhibit the mechanical properties of liquids or solids. Such physical material properties, classifying bilayer behavior with stress and strain rather than biochemical interactions, influence several membrane-mediated biological processes.<sup>7–11</sup> These properties are typically characterized in terms of the mechanical parameters: the area compression modulus  $K_a$ , a bending modulus  $K_b$ . The membranes of living cells have remarkable elastic physical properties,<sup>8,9</sup> which are believed to play a role in physiological processes. These elastic physical properties are closely related to the shape, stability, strength, and structural phases. Quantitative study of bending rigidity in different phases is also important for the applications. In particular, the values of  $K_a$  and  $K_b$  affect the ability of proteins and small molecules to insert into the bilayer.<sup>10,11</sup> Bilayer mechanical properties have also been shown to alter the function of mechanically activated ion channels.<sup>12</sup>

Even though the lipid bilayer itself is only about 4 nm thick, the diameters of liposomes and vesicles are an order of magnitude larger. Their sizes are generally in the range of 20 nm to 50  $\mu\text{m}$ . Roughly, small unilamellar vesicles (SUV) are typically below 100 nm, large unilamellar vesicles (LUV) are between 100 nm and 1  $\mu\text{m}$ , and giant unilamellar vesicles (GUV) are above 1  $\mu\text{m}$ . SUV and LUV are used to deliver different types of drugs while GUV is large enough to study with traditional fluorescence microscopy. The size of vesicles has important consequences on many physicochemical and biological properties, including the amount of entrapped volume per given amount of lipid, their biological fate, and the mechanism of clearance from blood.<sup>4</sup> For large vesicles, the bilayer properties do not depend on the curvature. For small vesicles, however, the membrane thickness is no longer negligible in comparison to the vesicle size and the inner and outer leaflets of the bilayer may behave differently. As a consequence, both the membrane characteristics and the bilayer mechanical properties may vary significantly with the vesicle size.

The preparation of liposomes generally results in vesicles with a wide range of sizes. To avoid measurements perturbed by polydispersity in vesicle size,<sup>13</sup> a solution of vesicles with uniform diameter is a prerequisite for studying size-dependent properties. In addition, the membrane characteristics and properties of SUV are not easily determined by available experimental techniques, although the structure and energetics of GUV can be explored by micropipet aspiration experiments. As a result, a theoretical approach based on molecular simulations may provide valuable microscopic insights and complement the deficiency of experimental studies on the behavior of vesicles.<sup>14</sup> In this paper, the size-dependent behavior associated with small unilamellar vesicles is investigated by dissipative particle dynamics simulations. First, vesicles of various sizes are assembled by model lipids via the change of lipid concentration. Second, the dependence of the membrane characteristics, such as membrane thickness, area

density, and orientation order, on the vesicle size is analyzed. Third, the lipid bilayer mechanics are explored by inflation and the influence of vesicle size on the material properties including area compression modulus and bending modulus are studied.

## II. MODEL AND SIMULATION METHOD

The dissipative particle dynamics (DPD) is a coarse-grained particle-based, mesoscale simulation technique that explicitly includes solvents and reproduces hydrodynamic behavior. Introduced by Hoogerbrugge and Koelman in 1992,<sup>15</sup> the DPD method combines some of the detailed description of the molecular dynamics (MD) but allows the simulation of hydrodynamic behavior in much larger, complex systems, up to the microsecond range. Like MD, DPD particles obey Newton's equation of motion<sup>16,17</sup>

$$\frac{d\mathbf{r}_i}{dt} = \mathbf{v}_i \quad \frac{d\mathbf{v}_i}{dt} = \mathbf{f}_i/m_i \quad (1)$$

where  $\mathbf{f}_i$  denotes the total forces acting on particle  $i$  with mass  $m_i$ .

**A. Interactions between Beads.** The interactions of the soft DPD beads are governed by three pairwise-additive, short-ranged forces: conservative ( $F^C$ ), dissipative ( $F^D$ ), and random forces ( $F^R$ )

$$\mathbf{f}_i = \sum_{j \neq i} \left( F_{ij}^C + F_{ij}^D + F_{ij}^R \right) \quad (2)$$

These forces conserve net momentum and all acts along the line joining two interacting particles. The conservative force  $F^C$  for nonbonded beads is a soft repulsive force

$$\mathbf{F}_{ij}^C = a_{ij}(r_c - r_{ij})\hat{\mathbf{r}}_{ij}, \quad r_{ij} \leq r_c; \quad 0, r_{ij} > r_c$$

where  $a_{ij}$  is a maximum repulsion between particles  $i$  and  $j$  and  $r_{ij}$  is the magnitude of the bead-bead vector.  $\hat{\mathbf{r}}_{ij}$  is the unit vector joining beads  $i$  and  $j$ . The interaction parameter  $a_{ij}$  can be qualitatively estimated based on the relationship between  $a$  and the Flory-Huggins parameter  $\chi$  established by Groot and Warren.<sup>16</sup> For fairly compatible species  $i$  and  $j$ ,  $a_{ij} \approx 25$ . As incompatibility between  $i$  and  $j$  increases,  $a_{ij}$  increases. The dissipative or drag force has the form

$$\mathbf{F}_{ij}^D = -\gamma w^D(r_{ij})(\hat{\mathbf{r}}_{ij} \cdot \mathbf{v}_{ij})\hat{\mathbf{r}}_{ij}$$

where  $\mathbf{v}_{ij} = \mathbf{v}_i - \mathbf{v}_j$  and  $w^D$  is an  $r$ -dependent weight function. The form is chosen to conserve the total momentum of each pair of particles and therefore the total momentum of the system is conserved. The dissipative force acts to reduce the relative momentum between particles  $i$  and  $j$ , while random force is to impel energy into the system. The random force also acts between all pairs of particles as

$$\mathbf{F}_{ij}^R = -\sigma \omega^R(r_{ij}) \theta_{ij} \hat{\mathbf{r}}_{ij} \quad (3)$$

where  $\sigma = (2\gamma k_B T)^{1/2}$  represents the noise amplitude,  $\omega^R$  is a  $r$ -dependent weight function, and  $\theta_{ij}$  is a randomly fluctuating variable whose average number is zero.

In this work, the model lipid is designated as  $A_3(B_6)_2$  where  $A$  is the hydrophilic head bead and  $B$  denotes the hydrophobic tail bead. Schematic diagram of the lipid is shown in Figure 1a. For the model lipid in this work, we also have to consider the interaction forces between bonded beads

$$\mathbf{F}_i^S = -\sum_j C^S(r_{ij} - r_{eq})\hat{\mathbf{r}}_{ij} \quad (4)$$

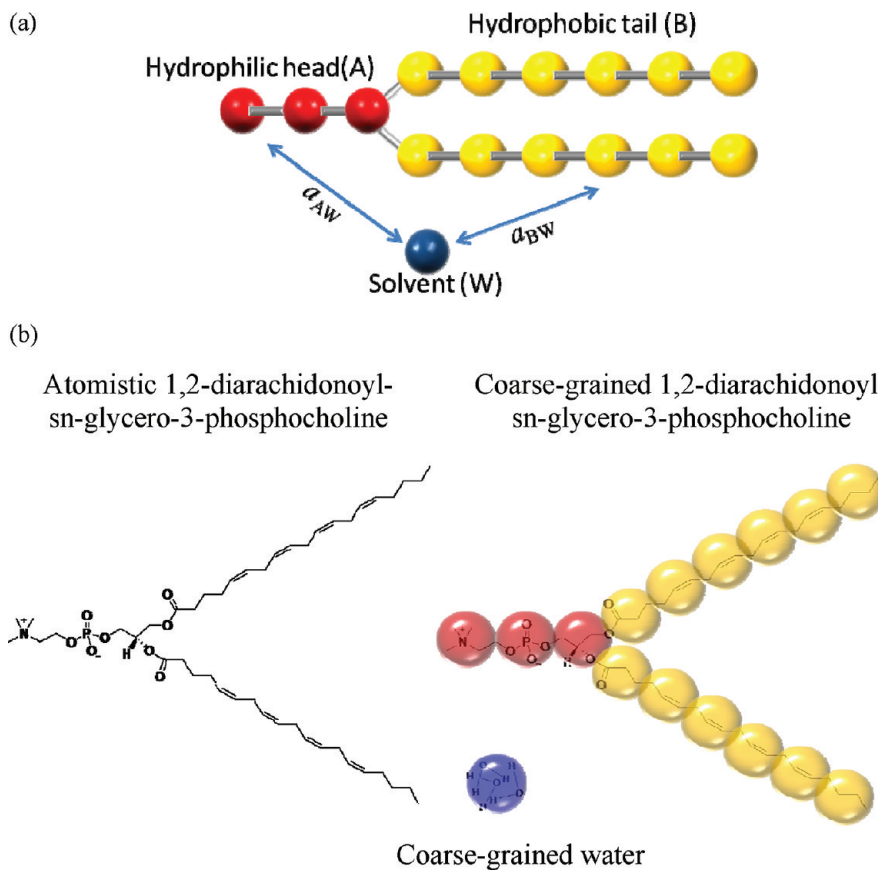


**Figure 1.** Schematic diagrams of (a) the model lipids ( $A_3(B_6)_2$ ) and their interactions with the solvents (W); (b) the mapping between the atomistic 1,2-diarachidonoyl-*sn*-glycero-3-phosphocholine and the coarse-grained 1,2-diarachidonoyl-*sn*-glycero-3-phosphocholine in DPD simulations.

where the sum runs over all particles to which particle  $i$  is connected.  $C^S$  is the spring constant and  $r_{eq}$  denotes the equilibrium bond length. Two additional forces are employed<sup>18–20</sup> to mimic the stiffness of unsaturated lipid tails. The first one is the bending force, which is given by defining a bending potential

$$U^\theta = k_\theta(\theta - \pi)^2 \quad \mathbf{F}^\theta = -\nabla U^\theta \quad (5)$$

This force tends to compel the bond angle between two consecutive bonds to be close to the value of  $\pi$ . However, the bending force alone cannot provide satisfactory stiff conformation of the polyunsaturated (multiple methylene-interrupted C=C bonds) lipid tail. Consequently, an additional spring force is also employed for the hydrophobic tail. The additional spring force ( $\mathbf{F}^S$ ) for the first and third beads in every three neighboring beads takes the form<sup>21</sup>

$$\bar{\mathbf{F}}_i^S = -\sum_j \bar{C}^S(r_{ij} - \bar{r}_{eq})\hat{\mathbf{r}}_i \quad (6)$$

We have chosen  $C^S = \bar{C}^S = 100$ ,  $r_{eq} = 0.7$ ,  $\bar{r}_{eq} = 2r_{eq} = 1.4$ ,  $k_\theta = 20$ . These choices of  $C^S$ ,  $k$ , and  $r_{eq}$  will not affect the qualitative behavior of the systems studied in this work. All the forces except for the bonded spring force come to zero outside a certain cutoff radius  $r_c$ .

**B. System Parameters.** On the basis of the interaction model described above, the dynamics of 648 000 DPD particles was simulated in a cubic box ( $60^3$ ) under periodic boundary conditions. Note that, in DPD simulations, all the units are scaled by the particle mass  $m$ , cutoff distance  $r_c$ , and thermal energy  $k_B T$ .

The equation of motion are integrated with a modified velocity Verlet algorithm<sup>16</sup> with  $\lambda = 0.65$  and  $\Delta t = 0.01$ . Since DPD simulation utilizes soft-repulsive potentials, the systems studied are allowed to evolve much faster than the “brute-force” molecular dynamics. Therefore, a typical DPD simulation needs only about  $(5–10) \times 10^4$  steps to equilibrate. In this work, each simulation takes at least  $1.5 \times 10^6$  steps and the first  $1 \times 10^6$  steps are for equilibration. The concentration of model lipids can be used to control the vesicle size. We have defined the segment (volume) fractions of lipid ( $\varphi_l$ ) in the solution as

$$\varphi_l = \frac{\text{total no. of lipid beads}}{\text{total no. of beads}} = \frac{n_l \times 15}{n_l \times 15 + n_w}$$

where  $n_w$  is number of water bead and  $n_l$  is the number of lipids in the system and each lipid contains a total of 15 beads.

In the system, the model lipids form vesicles in water medium, and thus there are three different species of DPD particles, including solvent (W), hydrophilic particle (A) of the lipid, and hydrophobic particle (B) of the lipid. Figure 1a shows the schematic diagram of a model lipid and their interactions with the water solvent. Our simulation models can correspond qualitatively to the atomistic lipid of 1,2-diarachidonoyl-*sn*-glycero-3-phosphocholine in water solvent. The mapping between the atomistic lipids and the coarse-grained  $A_3(B_6)_2$  lipids in our DPD simulations can be performed as follows. First, an isolated 1,2-diarachidonoyl-*sn*-glycero-3-phosphocholine was constructed by using Materials Studio’s polymer and simulation modeling software.<sup>22</sup> Then, it was assumed that the choline, phosphate, and

**Table 1. Interaction Parameters ( $a_{ij}$ ) for the Lipid in Water Systems<sup>a</sup>**

$a_{ij} (\chi_{ij})$	A (hydrophilic head)	B (hydrophilic tail)	W (water)
A (hydrophilic head)	25		
B (hydrophilic tail)	50 (5.99)	25	
W (water)	26 (0.47)	50 (7.93)	25

<sup>a</sup> The  $\chi_{ij}$  parameters estimated from the Blends module of Material Studio are also shown in the parentheses.

glycerol groups can be taken as a spherical bead with diameter equal to 5.8 Å, 5.9 Å, and 4.9 Å, respectively. The  $\alpha$ -butylene of the hydrophobic tail was estimated to have the size of approximately 5.5 Å and can be taken as one DPD bead. The water molecule has the size of approximately 1.51 Å, and therefore one DPD bead contains roughly three water molecules. Figure 1b demonstrates how 1,2-diarachidonoyl-*sn*-glycero-3-phosphocholine is mapped onto the “beads” described in the model.

The interaction parameters chosen are shown in Table 1. These repulsive interaction parameters ( $a_{ij}$ ) are not randomly selected. According to Groot and Warren,<sup>15</sup> the interaction parameter can be estimated from the Flory–Huggins  $\chi$ -parameter by their  $\chi-a$  relation:  $\chi_{ij} = (0.286 \pm 0.002)(a_{ij} - a_{ii})$ , where  $a_{ii} = 25$  for  $i = A, B, W$ . As one knows, it is difficult to acquire the  $\chi$  parameter of every pair of components from experiments. “Blends”, which is the module of Materials Studio from Accelrys Inc., provides a way to shorten the discovery process by estimating the miscibility behavior of binary mixtures.<sup>22</sup> It predicts the thermodynamics of mixing directly from the chemical structures of the two components and, therefore, requires only their molecular structures and a forcefield as inputs. Here, the COMPASS forcefield is used. The  $\chi$  parameters estimated from the Blends module are also shown in Table 1 and the interaction parameters can then be calculated by the  $\chi-a$  relation. Note that the interaction parameters are rounded to “cleaner” numbers as listed in Table 1. Nevertheless, the results should remain qualitatively unchanged.

There are several works providing chemically much more accurate coarse-grained models.<sup>23–26</sup> For example, in the work of Shelley and co-workers some potential parameters were fitted on the basis of comparisons with the results of a separate study of an atomistic simulation of a lipid bilayer.<sup>23</sup> Marrink et al. provided a coarse-grained model for semiquantitative lipid simulations.<sup>24</sup> Structural properties and elastic properties were found to match experimentally measured quantities closely. Kranenburg and Smit performed Molecular Dynamics simulations of a single lipid in water using a realistic all-atom representation to generate configurations of the lipid, which were subsequently used to optimize the intramolecular interactions.<sup>25</sup> Compared to these above-mentioned models, our approach seems to be less refined. Nevertheless, our intention is to develop a coarse-grained model that possesses characteristic physical and structural features of water and lipid system. The distinctive structural and mechanical properties can be qualitatively demonstrated.

### III. RESULTS AND DISCUSSION

The size-dependent properties of small vesicles, such as membrane tension and mechanical properties, are closely related to their bilayer characteristics, including membrane thickness, area densities of inner and outer leaflets, and order parameter. First, spherical vesicles with various sizes ( $r$ ) are spontaneously

formed by changing the volume fraction of model lipids ( $\varphi_l$ ). The membrane characteristics are then analyzed for different vesicle sizes. The membrane tension can be obtained by evaluating the pressures inside and outside the vesicle. Upon the inflation approach via liquid injection into the vesicle, the mechanical properties like stretching and bending moduli are determined as well. The variations of the membrane characteristics and mechanical properties with the vesicle size are shown and the results are compared to those of an infinitely extended membrane.

**A. Spontaneous Formation of Vesicles with Different Sizes.** In this study, the vesicles are formed from the model lipids  $A_3(B_6)_2$  in water medium. The vesicles are constructed in two steps as displayed in Figure 2. First, a bowl-like bilayer structure is artificially built. Second, DPD simulation is performed to equilibrate the system and a vesicle is formed spontaneously. The water beads can come in and out of the vesicle before the open hole closes up. The open holes with different initial sizes are constructed, and it is found that the final characteristics, e.g., the size and the membrane thickness, of the spontaneously formed vesicles are essentially the same, irrespective of the initial size of the open hole, as shown in Figure 2 for small and big holes. Note that, before vesicle enclosure, a large initial hole evolves into two holes during the equilibrating process, as depicted in Figure 2b. In the work of Markvoort et al.,<sup>27</sup> a similar procedure was adopted to form a vesicle. They also found that formation of vesicles is a nonequilibrium process. When the vesicle encapsulates solvent, the line tension of the remaining pore stretches the area of the bilayer because the ability for solvent to flux decreases as the pore closes. In other words, pore closure is faster than flux and the latter process gives rise to a pressure gradient which has readily been well described.<sup>27</sup>

As we have mentioned, small vesicles are less stable thermodynamically than the larger ones against fusion. This is attributed to their bilayer characteristics. To investigate the relation between vesicle sizes and membrane characteristics, vesicles with different radii are spontaneously formed by controlling the number of model lipids in the water medium. Since the box size remains the same throughout all simulations, the change in the number of model lipids corresponds to changes in volume fraction of lipids ( $\varphi_l$ ). In this work,  $\varphi_l$  of 0.015, 0.03, 0.045, 0.06, 0.075, 0.09, 0.12, and 0.15 are used. As depicted in Figure 3a, the radius ( $r$ ) of the spontaneously formed vesicle rises as  $\varphi_l$  is increased. Moreover, Figure 3b shows the snapshots of the spontaneously formed vesicles. The vesicles are sliced so that the inner regions are visible (note that solvent particles are not shown). Those vesicles are stable against fusion because they are isolated in a box.

It should be noted that the spontaneously formed vesicle is in a metastable state instead of a thermodynamic equilibrium state. After the equilibrating process of a closed vesicle, about 30 water beads are found to exchange between interior and exterior water domains and about 700 model lipids flip and flop between inner and outer leaflets for  $1.5 \times 10^5$  time steps in the system of  $\varphi_l = 0.09$ . There is no net change between the two domains and the two leaflets. As shown in Supporting Information Figure S1, the pressure and chemical potential of water beads remain essentially constant during the sampling period but the values in the interior domain are higher than those in the exterior domain. This consequence reveals that the vesicle is temporarily locked in a metastable state, which can persist for a long time. Note that the chemical potentials are calculated by Widom's test particle method.<sup>28</sup> This method has been

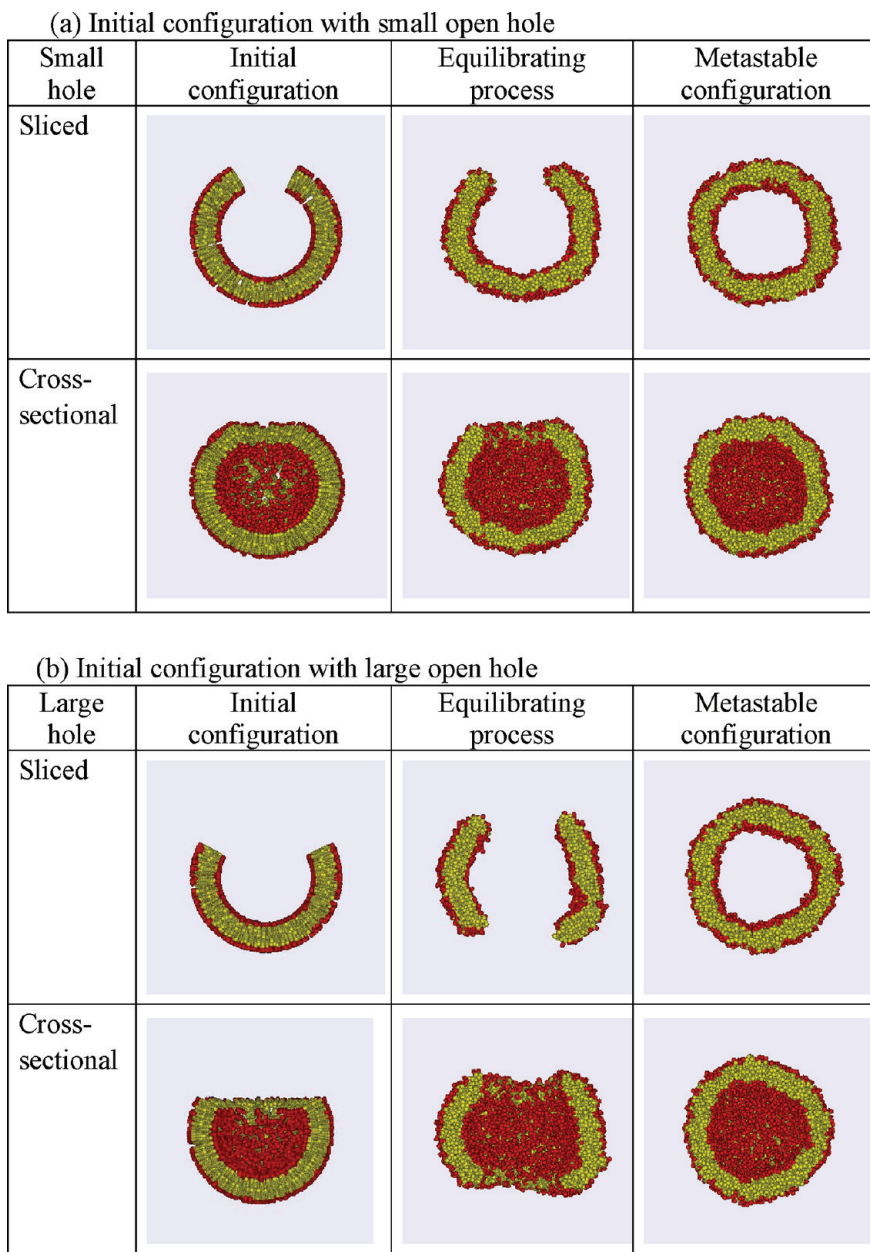


**Figure 2.** Evolutionary process of a vesicle with different initial configurations: (a) initial configuration with a small open hole; (b) initial configuration with a large open hole. The metastable states of the vesicles are essentially the same.

successfully applied to determine the chemical potentials of atomic and molecular fluids.<sup>29,30</sup>

**B. Membrane Characteristics (Lipid Packing and Orientation).** *1. Bilayer Thickness.* The membrane thickness is an important characteristic of the bilayer and closely related to its properties, such as permeability and bending modulus. Obviously, the membrane thickness depends on the length and degree of saturation of the fatty acid chain of which its lipids are made. Moreover, the lipid bilayer thickness plays an essential role in hydrophobic matching associated with lipid–protein interactions.<sup>2</sup> However, the membrane thickness may vary with the size of a vesicle assembled by a single lipid species only. As shown in Figure 4, the bilayer membrane is thinned by reducing the vesicle size. The cross-sectional slices of vesicles at different lipid volume fractions are demonstrated in Figure 4b. The membrane thickness

is determined from the difference between the outer and inner radii,  $h = r_o - r_i$ . Here, the outer or inner radii are defined as the average distance from the head of the lipid in the outer or inner leaflet to the center of mass of the vesicle, respectively. The vesicle size is then defined as the mean value of the outer and inner radii,  $r = (r_o + r_i)/2$ . It is interesting to find that the growth of the membrane thickness with increasing size can be approximately depicted by  $h(r) = h_\infty - V_{ex}/4\pi r^2$ , where  $h_\infty$  represents the thickness of an infinitely large membrane, i.e.,  $r \rightarrow \infty$ . As illustrated in the inset of Figure 4a, the plot of  $h$  against  $r^{-2}$  gives an intercept  $h_\infty$  and the value is consistent with the simulation result of a planar membrane formed by an appropriate initial configuration of model lipids. The slope implies that, at the same size  $r$ , the membrane volume of a fictitious vesicle made of the bilayer with  $h_\infty$  is always greater than that of a spontaneously

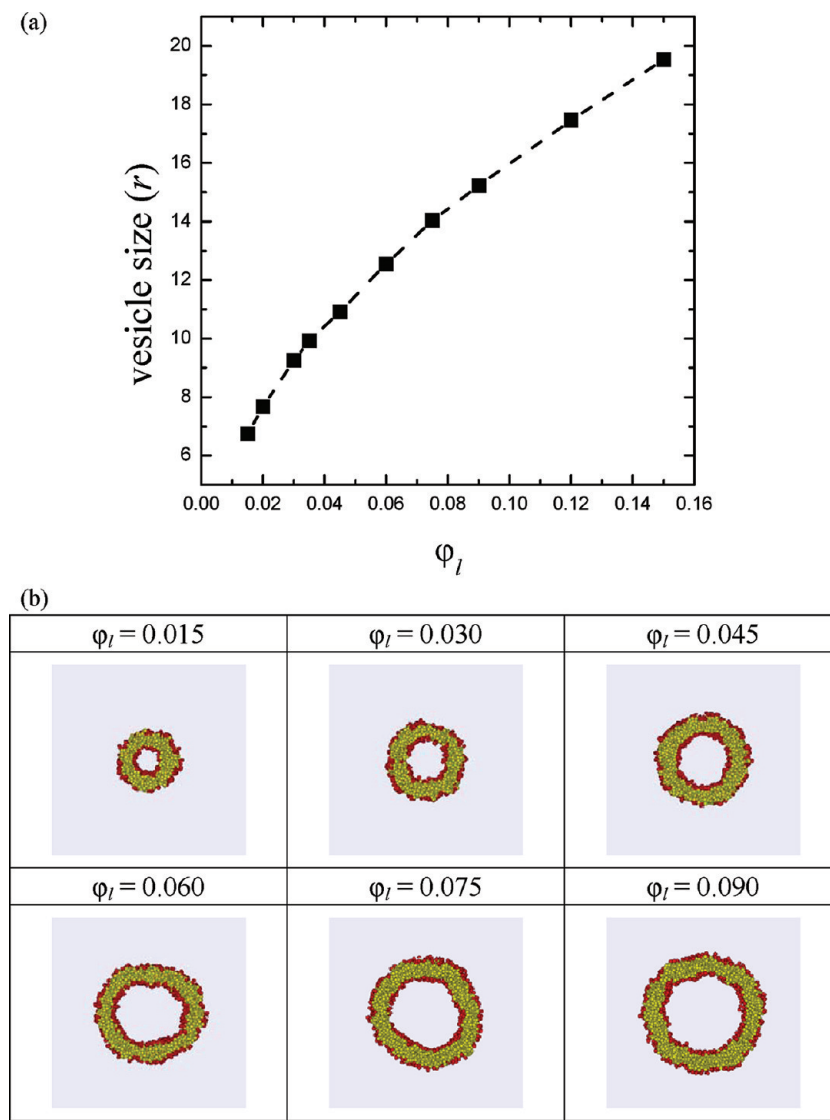


**Figure 3.** (a) Radius ( $r$ ) of the spontaneously formed vesicle versus the volume fraction of the lipids ( $\phi_l$ ). (b) Sliced images of the spontaneously formed vesicles.

formed vesicle by the excess volume  $V_{ex}$ . Supporting Information Figure S2 displays the cross-sectional snapshots of an infinitely large vesicle and some important physical properties.

**2. Area Density.** To understand the variation of the thickness with the vesicle size, the characteristics of lipid packing in the membrane are explored, including area densities ( $\sigma$ ), lipid lengths ( $l$ ), and lipid volumes ( $v$ ) in both leaflets. In many naturally occurring bilayers, the compositions of the inner and outer membrane leaflets are different, and thus, asymmetry in both leaflets arises. Nevertheless, the bilayer of a small unilamellar vesicle is asymmetric even though the inner and outer membrane leaflets are made of the same lipid. Figure 5 shows the variation of the area densities of the lipid head in both leaflets with the vesicle size. The outer and inner area densities are defined as  $\sigma_o^h = N_o / 4\pi r_o^2$  and  $\sigma_i^h = N_i / 4\pi r_i^2$ , respectively. Here,  $N_o$  and  $N_i$  depict the number of lipids in the outer and inner leaflets, respectively. Note that  $N_o$  is significantly larger than  $N_i$  in a small vesicle. Since the formation of vesicle has to bend the membrane, the inner face must be compressed and the outer face must be stretched. As a result, it is anticipated that the area

density of lipid head in the inner leaflet must be greater than that in the outer leaflet. Although both area densities rise with increasing the vesicle size, the area density in the inner leaflet is very close to that of an infinitely large membrane,  $\sigma_\infty$ , as indicated by the arrow in Figure 5. That is, the lipid heads on the inner side are crowded as a planar membrane but those on the outer side are uncrowded. On the contrary, the area density of the lipid tail on the outer side is as crowded as that of a planar membrane but that on the inner side is uncrowded. The area densities of lipid tails are defined as  $\sigma_i^t = N_i / 4\pi \bar{r}_i^2$  and  $\sigma_o^t = N_o / 4\pi \bar{r}_o^2$ , where  $\bar{r}$  represents the mean distance from the center of mass to the last bead of the tail and  $\bar{r}_o \approx \bar{r}_i \approx r$ . As the vesicle size is increased,  $\sigma_i^t$  grows while  $\sigma_o^t$  remains essentially the same as  $\sigma_\infty$ . Obviously, bending the membrane to form a closed vesicle leads to the compression of the tail of the outer leaflet and the headgroup of the inner leaflet. This aforementioned consequence reveals that the lipids on the outer side have a shape like a truncated cone while those on the inner side take the shape of an inverted truncated cone. Note that similar observations were already made in previous studies.<sup>31,32</sup> Through the analyses of the radial density profile,

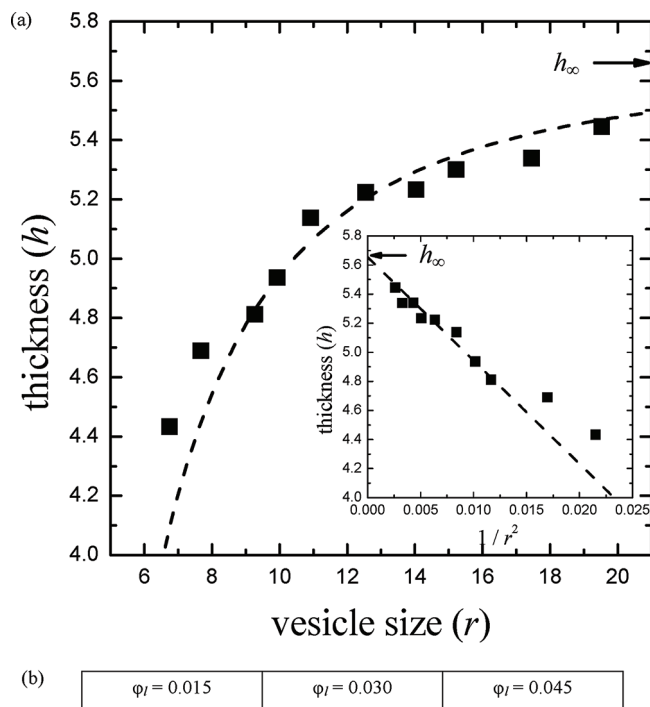


**Figure 4.** (a) Membrane thickness ( $h$ ) vs vesicle radius ( $r$ ). (b) Snapshots of the cross-sectional slices of vesicles at volume fractions ( $\phi_l$ ) of 0.015, 0.030, and 0.045. In the inset,  $h$  is plotted against  $r^{-2}$  and the intercept  $h_\infty$  agrees with the thickness of an infinitely large membrane indicated by the arrow.

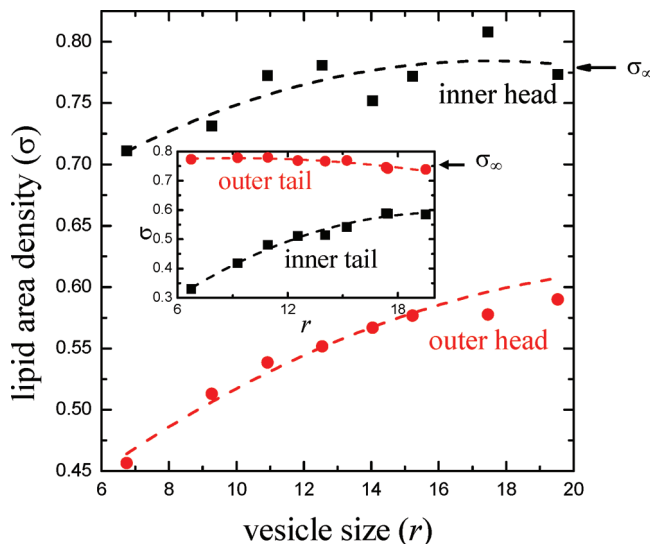


**Figure 5.** The lipid area density ( $\sigma$ ) versus vesicle size ( $r$ ) for both membrane leaflets, including inner head, outer head, inner tail, and outer tail.

they also found that the density in the headgroup area is larger in the inner monolayer than in the outer monolayer of the

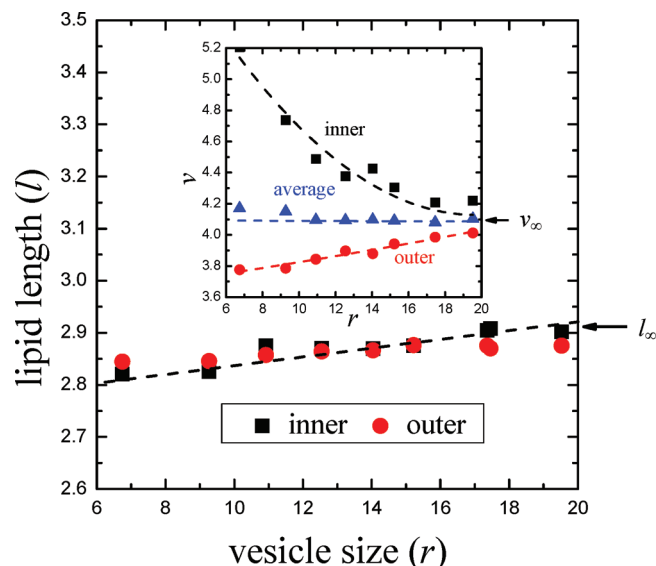


**Figure 6.** The lipid lengths ( $l$ ) of the inner and outer leaflets are plotted as a function of the vesicle size ( $r$ ). The lipid volumes ( $v$ ) of the inner and outer leaflets and the mean lipid volume of the membrane are shown in the inset.

liposome. In contrast, the density of the tails is larger in the outer monolayer than in the inner monolayer.

The area density of lipid head may influence the interfacial internal energy between apolar tails and polar medium (water and heads). Note that, similar to water, the lipid head likes water but dislikes the lipid tail, as depicted in Table 1. The shielding effect of the crowded heads of the inner layer results in a lower interfacial internal energy per lipid than that in the outer layer, i.e.,  $u_i < u_o$ , as shown in Supporting Information Figure S2. In addition, the interfacial internal energy in both outer and inner layers declines with increasing vesicle size. As indicated by the arrow,  $u_i$  approaches the interfacial internal energy associated with the planar membrane. This result is consistent with the variation of  $\sigma^h$  with  $r$  and indicates that the increment of the area density of lipid head can reduce the contacts between lipid tails and water significantly. At a given lipid volume fraction, there exists an optimal vesicle size corresponding to local minimum free energy of the system. When the size is perturbed, a smaller vesicle size increases the crowdedness of the inner layer while a larger size raises the interfacial energy of the outer layer. Both directions of size perturbation lead to the increment of the free energy.

**3. Packing Parameter.** Furthermore, we examine the lipid length and volume. As illustrated in Figure 6, the lipid lengths are essentially the same for both leaflets and rise weakly as  $r$  is increased. Since the lipid tail is quite rigid, the increment in length may be attributed to the extension of the headgroup. The mean lipid volume can be estimated by  $v_o = N_o/(4\pi/3)(r_o^3 - \bar{r}_o^3)$  and  $v_i = N_i/(4\pi/3)(\bar{r}_i^3 - r_i^3)$ . The lipid volume on the inner side is greater than that on the outer side and declines with increasing  $r$ . On the other hand,  $v_o$  grows and approaches the lipid volume of a planar membrane  $v_\infty$  as the vesicle size is increased. It should be noted that, as demonstrated in the inset of Figure 6, the mean lipid volume of the bilayer is independent of the vesicle size and it obeys the incompressible condition of the fluid. The consequence of  $v_i > v_o$  is somewhat surprising because stretch on the outer side and compression on the inner side should yield an

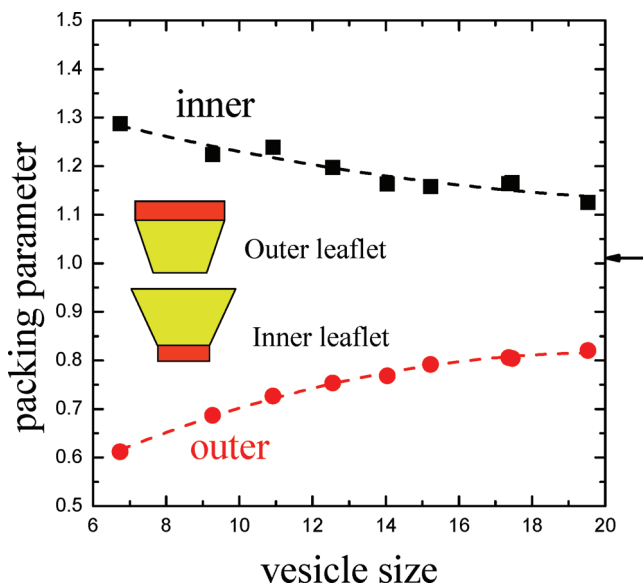


Figure 7. Packing parameters of the inner and outer leaflets are plotted as a function of the vesicle size.

opposite result. This fact reveals that lower lipid number density is required to reduce the crowdedness among lipid headgroups in the inner leaflet.

Evidently, the interfacial area per lipid exposed to the aqueous phase, i.e., optimal headgroup area  $a$ , is related to the area density by  $a = 1/\sigma^h$ . The packing shapes of the lipids and the structure they formed can be described by the dimensionless packing parameters, defined as  $\bar{P}_o = v_o/a_o l_o$  and  $\bar{P}_i = v_i/a_i l_i$  based on the geometric packing considerations. As illustrated in Figure 7, the packing parameter of the outer leaflet follows  $1/2 < \bar{P}_o < 1$  and grows with increasing  $r$ . On the other hand, the packing parameter of the inner leaflet obeys  $1 < \bar{P}_i$  and decays with increasing  $r$ . The former corresponds to the truncated cone while the latter indicates the inverted truncated cone or wedge as also shown in Figure 7. This consequence agrees with that inferred from the area densities,  $\sigma^h$  and  $\sigma^t$ . As  $r$  is increased, both  $\bar{P}_o$  and  $\bar{P}_i$  approach toward the packing parameter of a planar membrane,  $\bar{P}_\infty \sim 1$ .

**Lipid Orientation.** The membrane of a vesicle has a unilamellar structure. The description of liquid crystals involves an analysis of order. The orientational order of a liquid crystal is generally quantitatively described by the orientation order parameter. For a typical liquid crystal sample,  $S$  is on the order of 0.3 to 0.8. Since the local director, i.e., the preferred direction in a volume element of a liquid crystal sample, is absent in the bilayer membrane of a vesicle, the detailed packing arrangements within the spherical shell are expressed by the local order parameter associated with the hydrophobic lipid tails. The short-ranged order parameter is defined as<sup>20</sup>

$$S = \sum_{i=1}^{N_p} \sum_{j=1}^{N_i^*} \left( \frac{3 \cos \theta_{ij} - 1}{2} \right) / \sum_{i=1}^{N_p} N_i^* \quad (7)$$

where  $\theta_{ij}$  denotes the included angle between two neighboring hydrophobic tails as illustrated in Supporting Information Figure S4. The number  $N_i^*$  means the total number of neighboring hydrophobic tails around a centered tail  $i$  and is determined according to the schematic demonstration as shown in

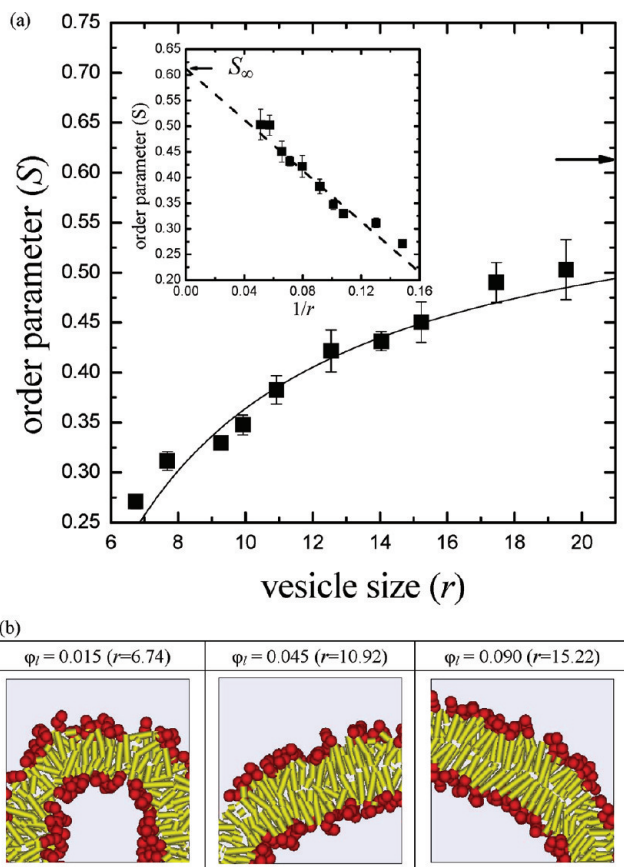


Figure 8. (a) Local order parameter ( $S$ ) versus vesicle radius ( $r$ ). (b) Cross-sectional slices of the snapshots for different vesicle sizes. In the inset,  $S$  is plotted against  $r^{-1}$  and the intercept  $S_\infty$  agrees with the local order parameter of an infinitely large membrane indicated by the arrow.

Figure Supporting Information S4(b).  $N_i^*$  can be determined by counting the total number of hydrophobic tails within the cylindrical domain of a centered lipid tail. The cylindrical domain is with radius  $l/2$  and length  $l$ , where  $l$  is the length of the lipid tail. Note that any hydrophobic tail with one or more beads situating within the cylindrical domain is counted as a neighboring hydrophobic tail around the centered lipid tail. As a consequence, the value of local order parameter  $S = 1$  represents that the neighboring hydrophobic tails are perfectly aligned in parallel and  $S = 0$  indicates an isotropic conformation.

As shown in Figure 8a, the local order parameter grows from 0.27 to 0.50 as the vesicle size increases. This result indicates that a much more ordered structure is formed for the large-sized vesicle. It is found that the variation of  $S$  with  $r$  can be expressed by the relation  $S = S_\infty - l^*/r$ . Evidently, the extrapolation of the order parameter to  $r = \infty$  by the plot of  $S$  against  $1/r$  yields  $S_\infty = 0.62$ , which is consistent with the order parameter associated with a planar membrane. The slope gives a characteristic length 2.48, which reveals the characteristic thickness of the leaflet ( $h/2$ ). The snapshots of the vesicles illustrated in Figure 8b confirm the calculated results. Note that the lipid tails are displayed in rods for demonstration purpose. As one can see, a nice bilayered arrangement takes shape for the large vesicle (i.e.,  $\phi_l = 0.090$ ,  $r = 15.22$ ). The rods are more or less orientating at the same direction to their close neighbors. As the vesicle becomes smaller in size, the bilayered formation is destructed. For the smallest

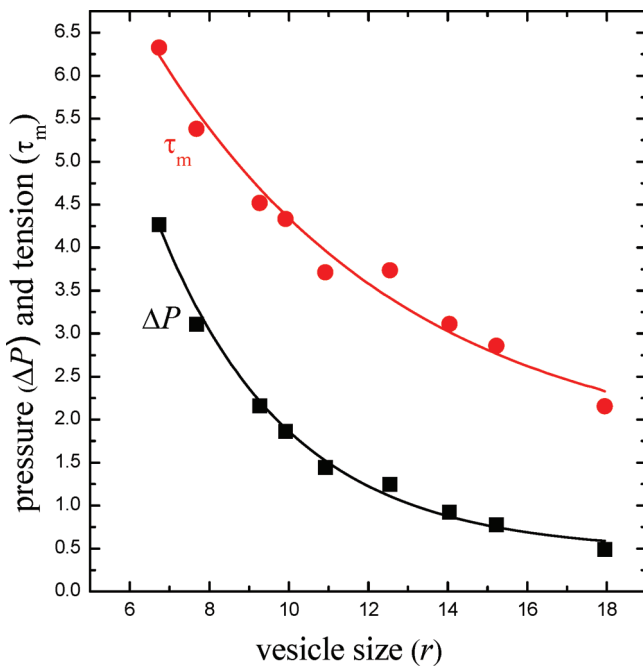


Figure 9. Membrane tension and pressure difference of the vesicle versus the vesicle size ( $r$ ).

vesicle studied in this case (i.e.,  $\varphi_l = 0.015$ ,  $r = 6.74$ ), some interdigitated conformations are developed.

The thinner membrane of a smaller vesicle reveals that the bilayer may have either an interdigitated structure or an orientational disorder conformation. In the latter case, lipids point away from the radial direction ( $e_r$ ), instead of parallel to  $e_r$ . If the angle between the lipid and  $e_r$  is denoted by  $\phi$ , the membrane thickness is about the addition of the inner and outer projection of lipids on  $e_r$ , i.e.,  $\langle l_o \cos \phi_o \rangle + \langle l_i \cos \phi_i \rangle$ , which is less than  $2l$ . As shown in Supporting Information Figure S5, one has  $\langle \cos \phi_o \rangle > \langle \cos \phi_i \rangle$  and both contributions grow with increasing vesicle size. According to the orientational order parameter, lipid tails do not parallel each other well. The area densities of tails and heads also reveals a shape of the truncated cone for lipids. Moreover, we have obtained the result of  $\bar{r}_o \geq \bar{r}_i$ . As a consequence, the thin bilayer of small vesicles can be mainly attributed to the orientational disorder. Figure 8b clearly demonstrates the scenario of such an orientational disorder.

**C. Mechanical Properties.** The mechanical characteristics affect how vesicles and their complexes encapsulate and deliver active agents. Some important mechanical properties can be obtained by analyzing the simulation results. The relationship between membrane tension and vesicular stability has been studied extensively.<sup>33</sup> In fact, the membrane tension of a vesicle has a significant impact on the fusion process. The membrane tension ( $\tau_m$ ) of a vesicle can be estimated by the Young-Laplace equation

$$P_i - P_o = 2\tau_m \left( \frac{1}{r_i} + \frac{1}{r_o} \right) \quad (8)$$

where  $P_i$  and  $P_o$  are pressures estimated in the inner and outer water regions of the vesicle, respectively. The radii of the curvature of the inner and outer interfaces associated with the spherical vesicle are represented by  $r_i$  and  $r_o$ , respectively. We assume the pressure in the membrane to be  $P_m$  and the interfacial

tensions on both sides are  $\gamma_i$  and  $\gamma_o$ , respectively. The combination of the two relations,  $P_i - P_m = 2\gamma_i/r_i$  and  $P_m - P_o = 2\gamma_o/r_o$  yields eq 8. Note that the assumption  $\gamma_i = \gamma_o = \tau_m$  has been made. It is also worth mentioning that the Young–Laplace equation is valid only when the Tolman length is small compared to the vesicle radius. Recently, the Tolman length can be estimated from the product of isothermal compressibility and tension. Since the compressibility in our system is about 1/48 and the tension is in the range of 2–6, the product of them is small compared to the vesicle radius 6–20. Therefore, the next order correction associated with the Tolman length can be neglected in our study.

For a vesicle, the pressures in the interior and exterior water domains of the vesicle can be estimated by the virial theorem. The membrane tension can then be calculated by eq 8 once the pressure difference and vesicular radii are obtained. Figure 9 shows the variation of pressure difference ( $\Delta P$ ) and membrane tension ( $\tau_m$ ) as a function of the vesicle radius ( $r$ ). It can be seen that the surface tension exhibits a declining trend as the size of a spontaneously formed vesicle increases. The membrane tension originates primarily from the interfacial tension between lipid tails and water. As the vesicle size is increased, the area density of lipid heads grows, the tail/water contact is reduced, and thereby the interfacial tension declines. This result reveals that a spontaneous formed vesicle with smaller size possesses comparatively larger membrane tension. As a consequence, small vesicles are less stable against fusion and destabilize immediately in order to reduce the tension as they are in contact with the other bilayers.<sup>34</sup>

In addition to membrane tension, the area stretching modulus  $K_a$  and the bending modulus  $K_b$  are the two important mechanical parameters in lipid bilayer mechanics. To study  $K_a$  and  $K_b$  of lipid bilayer, it must be curved in some measurable way with known and well characterized forces or moments. Thus, the two moduli are difficult to measure experimentally because of the thin, fragile nature of bilayers and the consequently low forces involved. One method utilized is to determine how vesicles swell in response to osmotic stress. In this work, we have used an inflation method to obtain the mechanical properties associated with a spontaneously formed vesicle. As water beads are injected into the interior water region of the vesicle, the vesicle size is increased. By measuring the inner and outer radii of the vesicle, the area dilation can be determined as  $\Delta A = A_s - A$ , where  $A$  is the surface area of the spontaneously formed vesicle and  $A_s$  represents the surface area of the swelled vesicle. The fractional change in the vesicle surface area is defined as  $\alpha = \Delta A/A$ . Owing to the addition of water beads into the internal water region of the vesicle, the inner pressure  $P_i$  and the volume of the vesicle grow. The outer pressure  $P_o$  remains roughly the same and therefore the membrane tension is expected to rise as the vesicle is swelled. As a result, one has the tension increment due to water addition,  $\Delta\tau_m = \tau_m^s - \tau_m$ . Figure 10 confirms this statement and displays the increase in membrane tension versus the fraction change in the surface area of the bilayer.

A general constitutive relation for elastic dilation of fluid bilayers was proposed<sup>35,36</sup>

$$\alpha = \frac{k_B T}{8\pi K_b} \ln \left( 1 + c \frac{A}{K_b} \Delta\tau_m \right) + \frac{\Delta\tau_m}{K_a} \quad (9)$$

where  $c$  is an unimportant constant of about 0.1 that depends on the type of modes (spherical harmonics or plane waves) used to describe surface undulations. Equation 9 can be used to extract

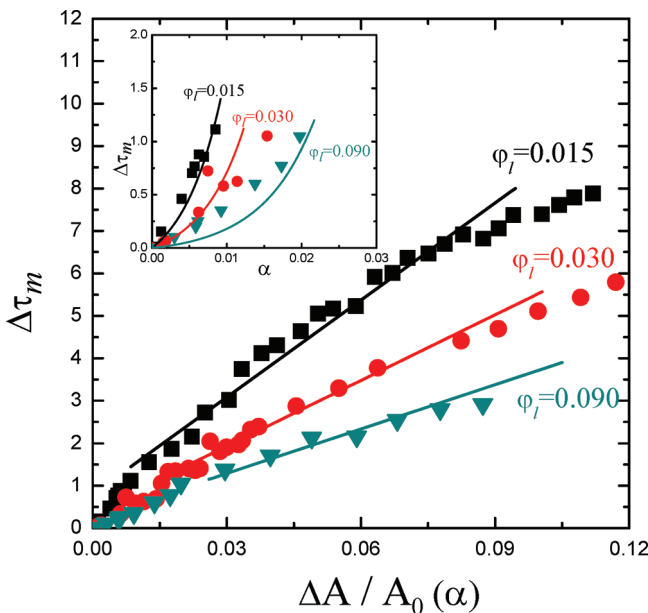


**Figure 10.** Tension increment ( $\Delta\tau_m$ ) is plotted against the fractional change in the vesicle surface area ( $\alpha$ ). The area stretching modulus can be obtained from the slope of  $\Delta\tau_m$  against  $\alpha$  for large area dilation. The bending modulus can be extracted from the small area dilation as shown in the inset.

the bending and stretching moduli. Ideally, both moduli can be obtained from a nonlinear fit of eq 9 to the data presented in Figure 10. For small area dilation ( $\alpha < 0.01$ ), the bending contribution dominates and the area is increased logarithmically with the tension

$$\alpha = \frac{k_B T}{8\pi K_b} \ln \Delta\tau_m + \text{const}$$

That is, the bending modulus can be extracted from the slope of  $\ln\Delta\tau_m$  against  $\alpha$ , as illustrated in the inset of Figure 10. For large area dilation, the stretching contribution prevails and the area grows linearly with the tension

$$\Delta\tau_m = K_a \alpha$$

The calculated bending and area stretching moduli for vesicles of different sizes are listed in Table 2. The typical value of  $K_b$  is about  $10-20 k_B T$ . Our simulation results of  $K_b$  ( $5.0-8.0 k_B T$ ) are slightly smaller but are well within the same order of magnitude. As one can see, the bending modulus declines gradually with increasing vesicle size. Different from  $K_b$ , the elastic area stretching modulus ( $K_a$ ) decreases quite significantly as the vesicle size is increased as shown in Table 2. Although our simulation results for large vesicles ( $\sim 100 k_B T/nm^2$ ) are consistent with the typical value of  $K_a \sim 70 k_B T/nm^2$ , the area stretch modulus of small vesicles can be more than twice the typical value. Here, the estimation is based on the bead size equal to 0.58 nm. This consequence indicates that more energy is needed to bend or stretch the membrane of smaller vesicle from its original large curvature. It can be realized by the higher membrane tension and the bilayer characteristics associated with the smaller vesicles.

In general, the bending modulus is dependent on the bilayer thickness. Due to the fact that to bend a bilayer, the inner face must be compressed and the outer face must be stretched, the bending modulus, area-stretch modulus and bilayer thickness are

**Table 2. Elastic Bending ( $K_b$ ) and Area Stretching ( $K_a$ ) Moduli for Various Vesicle Sizes**

$\varphi_1$	$r$	$K_b$	$K_a$	$h$	$K_b/(K_a h^2)$
0.015	6.74	7.58	76.22	4.43	0.0051
0.030	9.27	6.84	51.55	4.81	0.0057
0.045	10.92	6.62	47.56	5.14	0.0053
0.060	12.55	6.56	41.67	5.22	0.0057
0.075	14.04	6.14	38.57	5.24	0.0058
0.090	15.22	5.70	34.83	5.30	0.0058

generally related by

$$K_b = \beta K_a \cdot h^2 \quad (10)$$

where  $\beta \sim O(10^{-2})$ . This relation holds only for small deformations. If two of these parameters are known experimentally, the other can be calculated. If one assumes  $K_b \sim h^2$ , then the bending modulus should rise with increasing vesicle size. However, we have opposite results because all quantities  $K_a$ ,  $K_b$ , and  $h$  vary with the vesicle size. The change of the mechanical properties with the vesicle size can be comprehended by the fact that the membrane characteristics vary with the vesicle size as well. Therefore, one should examine whether the relation remains true under the same bilayer structure by evaluating  $K_b/K_a h^2$  for different values of  $r$ . In this work, it is found that this relation still holds for different vesicle sizes but the numerical constant,  $\beta = 5.6 \times 10^{-3}$  is smaller than the typical value.

**D. Simple Metastable Model.** We have shown that the spontaneously formed vesicles in DPD simulations are in a metastable state. As the vesicle size is reduced, the bilayer thickness declines while the membrane tension rises. It is interesting to find that there exists simple scaling expression for  $h$  and  $\tau_m$ . Here, a simple metastable model is proposed to explain such a size-dependent behavior. We assume that a thermodynamically equilibrium membrane has zero tension and the equilibrium area per lipid is  $a_\infty$ . When the hole of the vesicle is open, the tension is essentially zero and the pressure inside and outside the vesicle are equal. At the instant of the closure of the hole, the membrane tension and the inside pressure build up because the lipids are not enough for the formation of equilibrium vesicles. There are  $N$  lipids in this metastable vesicle with the size  $r$ . Its thickness  $h$  is thinner than the equilibrium value  $h_\infty$  but the area per lipid  $a$  is greater than  $a_\infty$ . Obviously, some surface areas are missing in order to bring the membrane to a state of zero-tension at the vesicle size  $r$ . Now, if we provide extra  $\Delta N$  lipids to the vesicle after it is formed, the area per lipid can be reduced to the equilibrium value  $a_\infty$ . As a consequence, the membrane would exhibit a zero-tension state, the bilayer thickness becomes  $h_\infty$ , but the vesicle size remains at  $r$ . Since the bilayer is incompressible, one has the volume difference between equilibrium and metastable vesicles

$$4\pi r^2 h_\infty = 4\pi r^2 h + \Delta N \cdot v_\infty$$

where  $v_\infty$  denotes the lipid volume. Therefore, one has

$$h = h_\infty - \left( \frac{\Delta N \cdot v_\infty}{4\pi} \right) \frac{1}{r^2} \quad (11)$$

As illustrated in Figure 4, the expression can depict the simulation result quite well with  $\Delta N \approx 165$ , which is independent of the vesicle size. This consequence implies that the vesicle

with an opening jumps to close up as the hole area reaches  $\Delta A = \Delta N \cdot a_\infty$ .

The orientation structure in terms of  $\langle \cos \phi \rangle$  can be estimated from the above result. Since  $h \approx 2l\langle \cos \phi \rangle$ , one has

$$\langle \cos \phi \rangle \approx \frac{h_\infty}{2l} - \left( \frac{\Delta N \cdot v_\infty}{8\pi l} \right) \frac{1}{r^2}$$

As depicted in the inset of Supporting Information Figure S5, the variation of  $\langle \cos \phi \rangle$  with  $r^{-2}$  can be described well by a linear line. The intercept representing the limiting value at  $r \rightarrow \infty$  agrees with the simulation result associated with a planar membrane. The variation of the membrane tension with the size of vesicle formed spontaneously can also be explained by the metastable model. According to the definition of area stretching modulus, one has  $\Delta \tau_m \sim (\Delta A/A)$ . The membrane tension is built up due to the area stretch instantly from a vesicle with an opening of area  $\Delta A$  to a closed one, which is metastable. Since  $\Delta N$  and  $a_\infty$  are independent of the vesicle size, the missing area ( $\Delta A$ ) for the formation of an equilibrium vesicle is a constant as well. As a result, one has

$$\Delta \tau_m \sim \Delta A/A \sim (\Delta N \cdot a_\infty) \frac{1}{r^2}$$

Again, this scaling expression can describe the simulation result well, as shown in Figure 9.

Note that, although the competition between line tension and surface tension is responsible for the enclosure of the vesicle with an open hole, it is very difficult to evaluate the dynamic line tension associated with a small vesicle. As pointed out in this manuscript, the mechanical properties are size-dependent. During the pore-closing process, both line tension and surface tension vary with the vesicle size. As a result, it is extremely difficult to extract such information from the simulation study of SUV. However, the line tension may be obtained from the pore-closing dynamics associated with a planar membrane with an open hole.

#### IV. CONCLUSION

The size-dependent behavior of small unilamellar vesicles is explored by DPD simulations, including the membrane characteristics and mechanical properties. DPD simulations can offer valuable microscopic insights and circumvent perturbation by size polydispersity in experiments. The size of spontaneously formed vesicles is controlled by the concentration of model lipids,  $A_3(B_6)_2$ , where A and B are the hydrophilic head bead and the hydrophobic tail bead, respectively. There are 648 000 DPD beads in the system and additional forces are employed to mimic the stiffness of lipid tails. The fusion between vesicles is avoided because of isolation.

Independent of the initial conditions, the spontaneously formed vesicles are in the metastable state. Although there exists an exchange of water beads across the bilayer and flip-flop of lipids in the membrane, the chemical potential and pressure are higher in the interior of the vesicle. Nonetheless, those thermodynamic quantities remain essentially unchanged during the DPD simulations. It is found that, as the size of metastable vesicles decreases, the bilayer thickness ( $h$ ) is getting thinner and the area density of lipid head declines as well. Nonetheless, the area densities ( $\sigma^h$ ) are different in the inner and outer leaflets. The area density is higher in the inner leaflet ( $\sigma_i^h > \sigma_o^h$ ) and it is close to the limiting value associated with a planar membrane. The

packing parameters ( $\bar{P}$ ) are calculated for both leaflets.  $\bar{P}_i > 1$  grows but  $1 > \bar{P}_o > 1/2$  declines with reducing the vesicle size. This result indicates that the shape of the lipid in the outer leaflet is like a truncated cone but that in the inner leaflet resembles an inverted truncated cone. To describe the orientational structure in the bilayer, a local order parameter is defined. The orientation order is found to decay with reducing vesicle size and this fact reveals that the thinner bilayer is mainly attributed to the orientation disorder.

Since the membrane characteristics vary with the vesicle size, it is anticipated that the mechanical properties of the bilayer depend on the vesicle size as well. The membrane tension can be obtained through the Young–Laplace equation by determining the interior and exterior pressures. It is found that the tension grows with reducing vesicle size. This fact reveals that small vesicles are less stable thermodynamically against fusion in order to reduce the tension. On the basis of the inflation method, which is similar to the osmosis swelling, the area stretching ( $K_a$ ) and bending ( $K_b$ ) moduli can be determined for various vesicle sizes and they are consistent with the typical values. As the vesicle size is reduced, those moduli are found to grow. That is, both  $K_a$  and  $K_b$  are dependent on the membrane thickness. Nonetheless, the general relation among the bending modulus, area stretching modulus, and bilayer thickness is still followed with a small numerical constant. Finally, a simple metastable model is proposed to explain the size-dependent behavior of bilayer thickness and tension.

#### ■ ASSOCIATED CONTENT

**S Supporting Information.** Additional figures as described in the text. This material is available free of charge via the Internet at <http://pubs.acs.org>.

#### ■ AUTHOR INFORMATION

##### Corresponding Author

\*E-mail: yjsheng@ntu.edu.tw and hktsao@cc.ncu.edu.tw.

#### ■ ACKNOWLEDGMENT

This research work is supported by National Science Council of Taiwan. Computing times, provided by the National Taiwan University Computer and Information Networking Center and National Center for High-performance Computing (NCHC) are gratefully acknowledged.

#### ■ REFERENCES

- (1) Jones, M. N.; Chapman, D. *Micelles, Monolayers, and Biomembranes*; Wiley: New York, 1995.
- (2) Mouritsen, O. G. *Life-as a matter of fat*, Springer: Berlin, 2004.
- (3) Israelachvili, J. *Intermolecular & Surface Forces*, 2nd ed.; Academic Press: New York, 1994.
- (4) Lasic, D. D. *Liposomes: from physics to applications*; Elsevier: New York, 1993.
- (5) Discher, B. M.; Won, Y. Y.; Ege, D. S.; Lee, J. C.; Bates, F. S.; Discher, D. E.; Hammer, D. A. *Science* **1999**, 284 (5417), 1143.
- (6) Nardin, C.; Hirt, T.; Leukel, J.; Meier, W. *Langmuir* **2000**, 16, 1035.
- (7) Boal, D. H. *Mechanics of the cell*; Cambridge University Press: Cambridge, UK, 2001.
- (8) Ou-Yang, Z. C.; Helfrich, W. *Phys. Rev. Lett.* **1987**, 59, 2486.
- (9) Lipowsky, R. *Nature* **1991**, 349, 475.

- (10) McIntosh, T. J.; Simon, S. A. *Annu. Rev. Biophys. Biomol. Struct.* **2006**, *35*, 177.
- (11) Garcia, M. L. *Nature* **2004**, *430*, 153.
- (12) Suchyna, T. M.; Tape, S. E.; Koeppen, R. E.; Andersen, O. S.; Sachs, F.; Gottlieb, P. A. *Nature* **2004**, *430*, 235.
- (13) Rutkowski, C. A.; Williams, L. M.; Haines, T. H.; Cummins, H. Z. *Biochemistry* **1991**, *30*, 5688.
- (14) Huang, K. C.; Lin, C. M.; Tsao, H. K.; Sheng, Y. J. *J. Chem. Phys.* **2009**, *130*, 245101.
- (15) Hoogerbrugge, P. J.; Koelman, J. *Europhys. Lett.* **1992**, *19*, 155.
- (16) Groot, R. D.; Warren, P. B. *J. Chem. Phys.* **1997**, *107*, 4423.
- (17) Espanol, P.; Warren, P. B. *Europhys. Lett.* **1995**, *30*, 191.
- (18) Lowe, C. P. *Europhys. Lett.* **1999**, *47*, 145.
- (19) Nakajima, T.; Hirao, K. *J. Chem. Phys.* **2006**, *124*, 184108.
- (20) Chou, S. H.; Tsao, H. K.; Sheng, Y. J. *J. Chem. Phys.* **2011**, *134*, 034904.
- (21) Lin, Y. L.; Chiou, C. S.; Kumar, S. K.; Lin, J. J.; Sheng, Y. J.; Tsao, H. K. *J. Phys. Chem. C* **2011**, *115*, 5566.
- (22) Accelrys Software Inc. (2008) *Materials Studio Release Notes, Release 4.4*; Accelrys Software Inc., San Diego, USA.
- (23) Shelley, J. C.; Shelley, M. Y.; Reeder, R. C.; Bandyopadhyay, S.; Klein, M. L. *J. Phys. Chem. B* **2001**, *105*, 4464.
- (24) Marrink, S. J.; de Vries, A. H.; Mark, A. E. *J. Phys. Chem. B* **2004**, *108*, 750.
- (25) Kranenburg, M.; Smit, B. *J. Phys. Chem. B* **2005**, *109*, 6553.
- (26) Shinoda, W.; DeVane, R.; Klein, M. L. *J. Phys. Chem. B* **2010**, *114*, 6836.
- (27) Markvoort, A. J.; Spijker, P.; Smeijers, A. F.; Pieterse, K.; van Santen, R. A.; Hilbers, P. A. J. *J. Phys. Chem. B* **2009**, *113*, 8731.
- (28) Widom, B. *J. Chem. Phys.* **1963**, *39*, 2808.
- (29) Sheng, Y. J.; Panagiotopoulos, A. Z.; Kumar, S. K.; Szleifer, I. *Macromolecules* **1994**, *27*, 400.
- (30) Smit, B.; Mooij, G. C. A. M.; Frenkel, D. *Phys. Rev. Lett.* **1992**, *68*, 3657.
- (31) Marrink, S. J.; Mark, A. E. *J. Am. Chem. Soc.* **2003**, *125*, 15233.
- (32) Risselada, H. J.; Marrink, S. J. *Phys. Chem. Chem. Phys.* **2009**, *11*, 2056.
- (33) Gao, L.; Lipowsky, R.; Shillcock, J. *Soft Matter* **2008**, *4*, 1208.
- (34) Vrhovnik, S. K.; Kristl, J. *J. Controlled Release* **1999**, *59*, 87.
- (35) Helfrich, W.; Servuss, R. M. *Nuovo Cimento D* **1984**, *3*, 137.
- (36) Rawicz, W.; Olbrich, K. C.; McIntosh, T.; Needham, D.; Evans, E. *Biophys. J.* **2000**, *79*, 328.